Electronic Supplementary Information (ESI)

The choice of ionic liquid ions to mitigate corrosion impacts: the influence of superbase cations and electron-donating carboxylate anions

Xin Li,[a] Xiaoyu Wang,[a] Haq Nawaz,[a] Jiankang Zhang,[a] Xiaomei Chen,[b] Peng Cheng,[a] Tingting You,*[a] Shri Ramaswamy [c] and Feng Xu *[a]

[a] Beijing Key Laboratory of Lignocellulosic Chemistry, Beijing Forestry University, Beijing, 100083, PR China

[b] College of Chemistry and Materials Science, Northwest University, Xi'an, 710127, PR China

[c] Department of Bioproducts and Biosystems Engineering, University of Minnesota, St. Paul, MN, 55108, USA

*Corresponding author: Tel.: +86-10-62337993. Fax: +86-10-62337993.

Email address: youtingting0928@bjfu.edu.cn (T.-T. You); xfx315@bjfu.edu.cn (F. Xu).

Keywords: *Ionic liquids; Electrochemical corrosion; Metallic materials; Temperature; Water content*

Results and discussion

Table S1 Corrosion dynamic parameters of 304SS in [DBUH][$CH_3CH_2OCH_2COO$] at 20 ℃ to 60 ℃

Entry	E_{corr} (V vs SCE)	j_{corr} (μA/cm^2)	β_c (V/dec)	β_a (V/dec)
D-304SS-20 ℃	-0.497±0.005	0.442±0.003	0.350±0.007	0.626±0.005
D-304SS-40 ℃	-0.674±0.004	0.487±0.003	0.175±0.006	0.612±0.003
D-304SS-60 ℃	-0.774±0.005	0.513±0.001	0.105±0.003	0.597±0.006

Table S2 EIS data of 304SS in [DBUH][$CH_3CH_2OCH_2COO$] at 20 ℃-60 ℃

Entry	R_s (Ω·cm^2)	C_p (F·cm^{-2})	R_p (Ω·cm^2)	*CPE*		R_{ct} (Ω·cm^2)
				Y_0 (Ω^{-1}cm^{-2}S^{-1})	n	
D-304SS-20 ℃	22784 ±159.23	(1.823±0.006) x 10^{-6}	1230.8 ±31.006	(2.620±0.004) x 10^{-5}	0.8144 ±0.0007	(26.69±0.012) x 10^5
D-304SS-40 ℃	4855.0 ±48.471	(9.707±0.003) x 10^{-6}	622.23 ±15.419	(2.827±0.003) x 10^{-5}	0.8005 ±0.0004	(10.64±0.010) x 10^5
D-304SS-60 ℃	851.73 ±21.553	(9.982±0.008) x 10^{-6}	468.19 ±10.143	(3.083±0.006) x 10^{-5}	0.7287 ±0.0002	(8.425±0.005) x 10^5

Table S3 Corrosion dynamic parameters of 304SS in [EMIM][Ac] at 20 ℃-60 ℃

Entry	E_{corr} (V vs SCE)	j_{corr} (μA/cm^2)	β_c (V/dec)	β_a (V/dec)
E-304SS-20 ℃	-0.533±0.005	1.162±0.005	0.254±0.003	0.520±0.004
E-304SS-40 ℃	-0.533±0.003	1.230±0.004	0.207±0.006	0.335±0.002
E-304SS-60 ℃	-0.774±0.006	1.427±0.002	0.193±0.001	0.346±0.004

Table S4 EIS data of 304SS in [EMIM][Ac] at 20 ℃-60 ℃

Entry	R_s Ω·cm^2	C_p F·cm^{-2}	R_p Ω·cm^2	*CPE*		R_{ct} Ω·cm^2
				Y_0/Ω^{-1}cm^{-2}S^{-1}	n	
E-304SS-20 ℃	455.99 ±20.168	(6.996±0.003) x 10^{-6}	86.962 ±6.331	(9.348±0.002) x 10^{-6}	0.8099 ±0.0010	(22.08±0.011) x 10^5
E-304SS-40 ℃	142.25 ±13.247	(9.489±0.004) x 10^{-6}	80.640 ±5.489	(1.263±0.001) x 10^{-5}	0.8089 ±0.0008	(17.77±0.010) x 10^5
E-304SS-60 ℃	61.187	(10.60±0.003)	79.864	(1.625±0.001)	0.7922	(8.389±0.005)

	±6.6690	x 10^{-6}	±5.011	x 10^{-5}	±0.0006	x 10^{5}

Table S5 Corrosion dynamic parameters of 304SS in [AMIM][Cl] at 20 ℃-60 ℃

Entry	E_{corr} (V vs SCE)	j_{corr} (μA/cm^2)	β_c (V/dec)	β_a (V/dec)
A-304SS-20 ℃	-0.156±0.002	1.069±0.006	0.255±0.001	0.633±0.007
A-304SS-40 ℃	-0.213±0.002	4.089±0.012	0.342±0.003	0.282±0.004
A-304SS-60 ℃	-0.440±0.003	6.558±0.014	0.478±0.003	0.104±0.002

Table S6 EIS data of 304SS in [AMIM][Cl] at 20 ℃-60 ℃

Entry	R_s Ω·cm^2	C_p F·cm^{-2}	R_p Ω·cm^2	*CPE*		R_{ct} Ω·cm^2
				Y_0/Ω^{-1}cm^{-2}S^{-1}	n	
A-304SS-20 ℃	3401.7 ±39.215	(6.566±0.006) x 10^{-6}	1486.3 ±10.997	(6.524±0.003) x 10^{-6}	0.8019 ±0.0011	(11.30±0.010) x 10^{5}
A-304SS-40 ℃	624.66 ±26.489	(6.998±0.008) x 10^{-6}	97.045 ±8.100	(3.039±0.001) x 10^{-5}	0.6991 ±0.0008	(4.447±0.003) x 10^{4}
A-304SS-60 ℃	157.79 ±10.803	(2.109±0.001) x 10^{-5}	96.863 ±7.964	(4.051±0.002) x 10^{-5}	0.6833 ±0.0008	(3.505±0.001) x 10^{4}

Table S7 Corrosion dynamic parameters of 304SS in various water contents of [DBUH][$CH_3CH_2OCH_2COO$] electrolytes at 20 ℃

Entry	E_{corr} (V vs SCE)	j_{corr} (μA/cm^2)	β_c (V/dec)	β_a (V/dec)
D-304SS-0	-0.497±0.005	0.442±0.003	0.350±0.007	0.626±0.005
D-304SS-5%	-0.619±0.005	0.291±0.001	0.190±0.002	0.377±0.004
D-304SS-10%	-0.638±0.005	0.203±0.002	0.123±0.001	0.491±0.005
D-304SS-15%	-0.605±0.004	0.337±0.003	0.134±0.001	0.534±0.004
D-304SS-20%	-0.591±0.004	0.479±0.003	0.125±0.002	0.372±0.002

Table S8 EIS data of 304SS in various water contents of [DBUH][$CH_3CH_2OCH_2COO$] electrolytes at 20 ℃

Entry	R_s (Ω·cm^2)	C_p (F·cm^{-2})	R_p (Ω·cm^2)	*CPE*		R_{ct} (Ω·cm^2)
				Y_0 (Ω^{-1}cm^{-2}S^{-1})	n	

D-304SS-0	22784 ±159.23	(1.823±0.006) x 10^{-6}	1230.8 ±31.006	(2.620±0.004) x 10^{-5}	0.8144 ±0.0007	(26.69±0.012) x 10^{5}
D-304SS-5%	3102.7 ±36.844	(1.786±0.005) x 10^{-6}	1332.2 ±15.390	(2.347±0.002) x 10^{-5}	0.8238 ±0.0010	(28.77±0.020) x 10^{5}
D-304SS-10%	1488.9 ±29.006	(1.173±0.006) x 10^{-6}	2063.5 ±16.952	(1.922±0.001) x 10^{-5}	0.8886 ±0.0012	(35.66±0.026) x 10^{5}
D-304SS-15%	462.12 ±20.571	(6.492±0.002) x 10^{-6}	1142.8 ±10.846	(3.010±0.003) x 10^{-5}	0.8762 ±0.0009	(31.60±0.021) x 10^{5}
D-304SS-20%	281.28 ±18.812	(7.117±0.006) x 10^{-6}	552.47 ±6.1515	(3.321±0.003) x 10^{-5}	0.8697 ±0.0012	(29.10±0.025) x 10^{5}

Table S9 Corrosion dynamic parameters of 304SS in various water contents of [EMIM][Ac] electrolytes at 20 ℃

Entry	E_{corr} (V vs SCE)	j_{corr} (μA/cm^2)	β_c (V/dec)	β_a (V/dec)
E-304SS-0	-0.533±0.005	1.162±0.005	0.254±0.003	0.520±0.004
E-304SS-5%	-0.474±0.004	1.009±0.008	0.138±0.001	0.556±0.003
E-304SS-10%	-0.462±0.003	1.453±0.009	0.133±0.001	0.186±0.001
E-304SS-15%	-0.421±0.003	1.580±0.007	0.214±0.003	0.409±0.002
E-304SS-20%	-0.611±0.005	1.682±0.009	0.266±0.002	0.314±0.003

Table S10 EIS data of 304SS in various water contents of [EMIM][Ac] electrolytes at 20 ℃

Entry	R_s Ω·cm^2	C_p (F·cm^{-2})	R_p (Ω·cm^2)	*CPE*		R_{ct} Ω·cm^2
				Y_0/Ω^{-1}cm^{-2}S^{-1}	n	
E-304SS-0	455.99 ±20.168	(6.996±0.003) x 10^{-6}	86.962 ±6.331	(9.348±0.002) x 10^{-6}	0.8099 ±0.0010	(22.08±0.011) x 10^{5}
E-304SS-5%	197.18 ±20.030	(6.760±0.006) x 10^{-6}	300.33 ±5.2645	(8.388±0.005) x 10^{-6}	0.8379 ±0.0010	(36.53±0.031) x 10^{5}
E-304SS-10%	145.34 ±15.856	(1.058±0.001) x 10^{-5}	151.13 ±2.8944	(1.559±0.001) x 10^{-5}	0.8309 ±0.0011	(33.27±0.026) x 10^{5}
E-304SS-15%	90.717 ±8.1664	(1.176±0.001) x 10^{-5}	99.766 ±1.5562	(1.576±0.001) x 10^{-5}	0.8236 ±0.0010	(30.08±0.024) x 10^{5}
E-304SS-20%	77.154 ±6.1895	(1.372±0.002) x 10^{-5}	66.691 ±0.8863	(2.061±0.002) x 10^{-5}	0.8102 ±0.0011	(18.16±0.017) x 10^{5}

Table S11 Corrosion dynamic parameters of 304SS in various water contents of [AMIM][Cl] electrolytes at 20 ℃

Entry	E_{corr} (V vs SCE)	j_{corr} (μA/cm^2)	β_c (V/dec)	β_a (V/dec)
A-304SS-0	-0.156±0.002	1.069±0.006	0.255±0.001	0.633±0.007
A-304SS-5%	-0.422±0.005	5.322±0.026	0.257±0.003	0.319±0.003
A-304SS-10%	-0.426±0.004	5.800±0.034	0.281±0.003	0.327±0.003
A-304SS-15%	-0.428±0.004	7.779±0.039	0.295±0.004	0.309±0.003
A-304SS-20%	-0.700±0.006	35.58±0.254	0.196±0.001	0.507±0.004

Table S12 EIS data of 304SS in various water contents of [AMIM][Cl] electrolytes at 20 ℃

Entry	R_s Ω·cm^2	C_p (F·cm^{-2})	R_p (Ω·cm^2)	*CPE*		R_{ct} Ω·cm^2
				Y_0/Ω^{-1}cm^{-2}S^{-1}	n	
A-304SS-0	3401.7 ±39.215	(6.566±0.006) x 10^{-6}	1486.3 ±10.997	(6.524±0.003) x 10^{-6}	0.8019 ±0.0011	(11.30±0.010) x 10^5
A-304SS-5%	57.617 ±3.3469	(6.894±0.005) x 10^{-6}	940.43 ±9.0021	(2.493±0.001) x 10^{-5}	0.8244 ±0.0010	(2.335±0.005) x 10^5
A-304SS-10%	507.81 ±26.389	(7.676±0.005) x 10^{-6}	39.528 ±2.7089	(2.841±0.002) x 10^{-5}	0.8159 ±0.0011	(1.328±0.001) x 10^5
A-304SS-15%	126.67 ±10.741	(9.053±0.006) x 10^{-6}	36.012 ±1.9263	(4.309±0.002) x 10^{-5}	0.7618 ±0.0009	(1.067±0.001) x 10^5
A-304SS-20%	36.993 ±1.9661	(2.186±0.001) x 10^{-5}	27.233 ±1.2045	(6.174±0.003) x 10^{-5}	0.6991 ±0.0008	(6.452±0.002) x 10^4

Table S13 Elemental surface composition of original 304SS and 304SS after the polarization tests performed in 100 g [AMIM][Cl] at 60 ℃ (A-304SS-60 ℃) and 80 g [AMIM][Cl]/20 g water at 20 ℃ (A-304SS-20%)

Sample	Element (at.%)				
	C	O	N	Cl	Fe
304SS	69.26	22.46	1.55	0.00	6.73
A-304SS-60 ℃	60.64	34.64	3.62	0.17	0.93

A-304SS-20%	55.65	36.14	3.83	0.99	3.39

Table S14 Corrosion dynamic parameters of five metallic materials in [DBUH][$CH_3CH_2OCH_2COO$] at 20 ℃

Entry	E_{corr} (V vs SCE)	j_{corr} (μA/cm^2)	β_c (V/dec)	β_a (V/dec)
D-316SS-20 ℃	-0.425±0.003	0.355±0.002	0.258±0.001	0.618±0.005
D-304SS-20 ℃	-0.497±0.005	0.442±0.003	0.350±0.007	0.626±0.005
D-0Cr13FSS-20 ℃	-0.695±0.005	0.643±0.003	0.154±0.001	0.476±0.005
D-Q235CS-20 ℃	-0.549±0.005	0.517±0.004	0.283±0.002	0.675±0.006
D-20#CS-20 ℃	-0.502±0.004	0.481±0.003	0.339±0.003	0.726±0.006

Table S15 EIS data of five metallic materials in [DBUH][$CH_3CH_2OCH_2COO$] at 20 ℃

Entry	R_s (Ω·cm^2)	C_p (F·cm^{-2})	R_p (Ω·cm^2)	*CPE*		R_{ct} (Ω·cm^2)
				Y_0 (Ω^{-1}cm^{-2}S^{-1})	n	
D-316SS-20 ℃	73839 ±274.01	(1.554±0.005) x 10^{-6}	2128.6 ±25.315	(1.449±0.002) x 10^{-5}	0.8305 ±0.0008	(28.93±0.013) x 10^5
D-304SS-20 ℃	22784 ±159.23	(1.823±0.006) x 10^{-6}	1230.8 ±31.006	(2.620±0.004) x 10^{-5}	0.8144 ±0.0007	(26.69±0.012) x 10^5
D-0Cr13FSS-20 ℃	32676 ±183.55	(9.000±0.011) x 10^{-6}	664.55 ±7.2979	(3.081±0.005) x 10^{-5}	0.7839 ±0.0006	(6.919±0.004) x 10^5
D-Q235CS-20 ℃	21066 ±144.16	(7.771±0.009) x 10^{-6}	754.71 ±6.4187	(2.811±0.004) x 10^{-5}	0.7958 ±0.0007	(10.74±0.007) x 10^5
D-20#CS-20 ℃	36936 ±167.27	(6.483±0.008) x 10^{-6}	952.34 ±7.9912	(2.647±0.005) x 10^{-5}	0.8064 ±0.0008	(12.09±0.009) x 10^5

Table S16 Calculated quantum chemical parameters of [DBUH][$CH_3CH_2OCH_2COO$], [EMIM][Ac], and [AMIM][Cl]

Parameters	[DBUH][$CH_3CH_2OCH_2COO$]	[EMIM][Ac]	[AMIM][Cl]
E_{HOMO}/eV	-5.650	-5.570	-5.790
E_{LUMO}/eV	-1.080	-0.480	-0.690
ΔE/eV	4.570	5.090	5.100
μ/Debye	4.603	3.733	3.431
χ/eV	3.365	3.025	3.240

γ/eV	2.285	2.545	2.550
ΔN	0.795	0.781	0.737
I/eV	5.650	5.570	5.790
E/eV	1.080	0.480	0.690
σ/eV^{-1}	0.438	0.393	0.392
ω/eV^{-1}	2.478	1.798	2.058

Analysis details of XPS spectra

XPS technique was used to investigate the composition of the protective adsorbed layer on the surface of 304SS in [AMIM][Cl] at 60 ℃ and [AMIM][Cl] with the water content of 20% at 20 ℃. As expected in Fig. S1, the XPS wide scans of each sample displayed three major peaks at 711.1 eV, 530.2 eV, and 284.0 eV corresponding to the Fe 2p, O 1s, and C 1s, respectively.[1] For the samples A-304SS-60 ℃ and A-304SS-20%, new peaks were observed at binding energies of 397 eV.1 (N 1s) and 196.0 eV (Cl 2p), supporting the surface film generally comprised of iron oxides, chlorides, hydroxides, and residual [AMIM][Cl].[2] In this way, the high-resolution peaks for Fe 2p, Cl 2p, O 1s, and N 1s of 304SS surface after the polarization tests performed in [AMIM][Cl] and aqueous solutions are recorded, as shown in Fig. S2.

It can be found that the high-resolution XPS spectra of Fe 2p3/2 as depicted in Fig. S2 (a1) and (a2) showed four peaks. The peaks located at 709.2 eV and 710.9 eV were assigned to ferrous compounds and ferric compounds, respectively, such as FeClx (i.e., Fe^{2+} chloride and/or Fe^{3+} chloride), FeOOH (i.e., oxyhydroxide), Fe_2O_3 (i.e., Fe^{3+} oxide), and/or Fe_3O_4 (i.e., Fe^{2+}/Fe^{3+} mixed oxide).[1] The corresponding peak of the Fe(III) satellite occurred at 713.0 eV, while a peak emerged at 707.0 eV can be

ascribed to metallic Fe in the substrate.[2] These results revealed that the corrosion products covering the 304SS surface were mainly composed of iron oxide, chlorides, and hydroxides either in the [AMIM][Cl] or its aqueous mixture. Moreover, the surface of 304SS produced more ferric compounds in the aqueous solution of [AMIM][Cl] than that in separate [AMIM][Cl]. The above finding can also be verified from the Cl 2p and O 1s of XPS spectra in Fig. S2 (b1), (b2), (c1), and (c2). In the spectra of Cl 2p, a large peak appeared at 198.3 eV can be attributed to Cl^-, and the peak for $FeCl_3$ occurred at 199.6 eV, which suggested that the Cl^- was largely adsorbed on the 304SS surface in [AMIM][Cl] and its aqueous solution.[2] Besides, the O 1s spectrum was fitted by two peaks. The first peak occurred at 529.0 eV was attributed to O^{2-}. The second peak located at 530.5 eV referred to the oxygen in hydrous iron oxides, such as FeOOH and/or $Fe(OH)_3$.[1] Fig. S2 (d1) and (d2) showed the profiles of XPS spectra for N 1s. the signal at about 399.7 eV can be assigned to the presence of amine group (NR_3) on the 304SS surface, and the peak at 397.8 eV can be ascribed to the C-N-metal bond.[2, 3] These facts confirmed that the [AMIM][Cl] really remained on the surface of 304SS.

Hence, from the XPS results, it can be concluded that the corrosion product films adsorbed on the 304SS surface not only contained iron oxides, chlorides, and hydroxides, but also adhered to the residual electrolytes [AMIM][Cl].

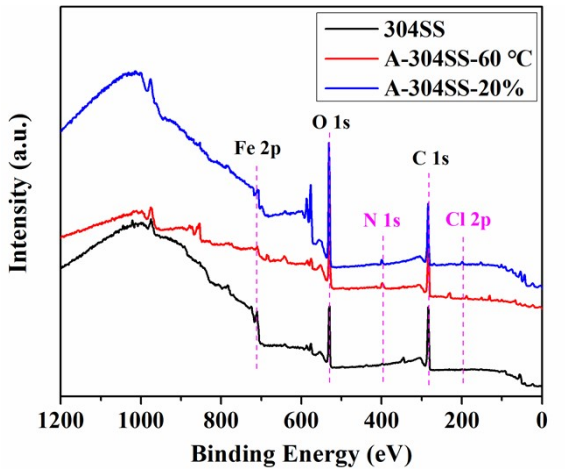

Fig. S1 XPS wide-scan spectra of 304SS surface before (304SS) and after the polarization tests performed in 100 g [AMIM][Cl] at 60 ℃ (A-304SS-60 ℃) and 80 g [AMIM][Cl]/20 g water at 20℃ (A-304SS-20%).

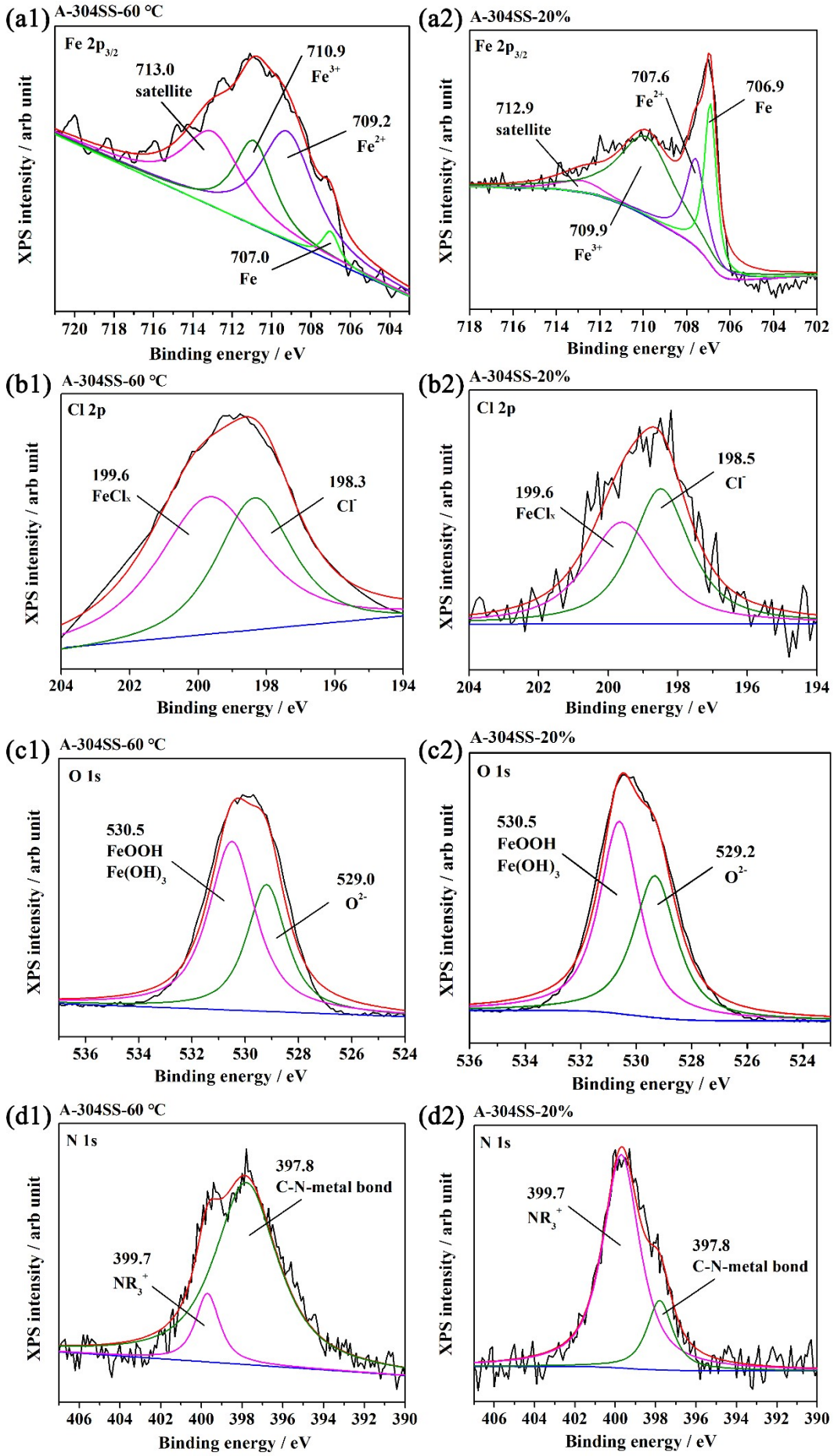
(a1)
A-304SS-60 ℃
Fe 2p3/2
713.0
satellite
710.9
Fe3+
709.2
Fe2+
707.0
Fe
XPS intensity / arb unit
720 718 716 714 712 710 708 706 704
Binding energy / eV
(a2)
A-304SS-20%
Fe 2p3/2
712.9
satellite
707.6
Fe2+
706.9
Fe
709.9
Fe3+
XPS intensity / arb unit
718 716 714 712 710 708 706 704 702
Binding energy / eV
(b1)
A-304SS-60 ℃
Cl 2p
199.6
FeClx
198.3
Cl-
XPS intensity / arb unit
204 202 200 198 196 194
Binding energy / eV
(b2)
A-304SS-20%
Cl 2p
199.6
FeClx
198.5
Cl-
XPS intensity / arb unit
204 202 200 198 196 194
Binding energy / eV
(c1)
A-304SS-60 ℃
O 1s
530.5
FeOOH
Fe(OH)3
529.0
O2-
XPS intensity / arb unit
536 534 532 530 528 526 524
Binding energy / eV
(c2)
A-304SS-20%
O 1s
530.5
FeOOH
Fe(OH)3
529.2
O2-
XPS intensity / arb unit
536 534 532 530 528 526 524
Binding energy / eV
(d1)
A-304SS-60 ℃
N 1s
397.8
C-N-metal bond
399.7
NR3+
XPS intensity / arb unit
406 404 402 400 398 396 394 392 390
Binding energy / eV
(d2)
A-304SS-20%
N 1s
399.7
NR3+
397.8
C-N-metal bond
XPS intensity / arb unit
406 404 402 400 398 396 394 392 390
Binding energy / eV

Fig. S2 High-resolution XPS for sample A-304SS-60 ℃ and A-304SS-20%: (a1) (a2) Fe 2p3/2; (b1) (b2) Cl 2p; (c1) (c2) O 1s; (d1) (d2) N 1s.

Experimental

Synthesis of [DBUH][$CH_3CH_2OCH_2COO$]

[DBUH][$CH_3CH_2OCH_2COO$] was synthesized by acid-base neutralization described in our previous work.[4] Under a nitrogen atmosphere, 1 mol DBU was added to n-hexane (1:3 mass ratio) followed by slow addition of 0.95 mol of the ethoxyacetic acid. The temperature of the reaction was controlled under 30 °C and left the reaction mixture under magnetic stirring for 12 h. The [DBUH][$CH_3CH_2OCH_2COO$] precipitated out of the n-hexane, leaving the residual DBU in the n-hexane. The obtained [DBUH][$CH_3CH_2OCH_2COO$] was repeatedly washed with n-hexane and separated. The high purity [DBUH][$CH_3CH_2OCH_2COO$] was obtained by drying at 80 ℃ for 1 h under nitrogen flow.

Table S17 Chemical compositions of five metallic materials (wt. %)

Element	316SS	304SS	0Cr13FSS	Q235CS	20#CS
C	≤0.08	≤0.08	≤0.08	≤0.20	0.17-0.23
Si	≤1.00	≤1.00	≤1.00	≤0.35	0.17-0.37
Mn	≤2.00	≤2.00	≤1.00	≤1.4	0.35-0.65
P	≤0.035	≤0.045	≤0.035	≤0.045	≤0.035
S	≤0.030	≤0.030	≤0.030	≤0.045	≤0.035
Cr	16.0-18.5	18.0-20.0	11.5-13.5	-	≤0.15
Mo	2.0-3.0	-	-	-	-
Ni	10.0-14.0	8.0-10.5	-	-	≤0.30
Cu	-	-	-	-	≤0.25

Corrosion characteristics

After the polarization measurements, the WE were thoroughly cleaned with anhydrous alcohol and then dried in cool air. Their surface morphologies and chemical compositions were investigated by Zeiss Merlin SEM equipped with an EDS. The acceleration voltage was 15 kV. Besides, the surface analysis was also conducted by XPS (Kratos AXIS SUPRA) with a monochromatic AI Kα X-ray source (1486.6 eV).

Theoretical calculations

Density functional theory (DFT) calculations with Gaussian 09 program suite and Multiwfn program were executed to elucidate the reactive centers of three ILs. All samples were subjected to optimize the geometry and present quantum chemical parameters using the B3LYP exchange-correlation function combined with the 6-31+G* basis set. The dipole moment of the molecule was calculated using more accurate method m062x/def2-TZVPD because diffusion function is very import for polarization related calculations. The visualization of the frontier orbitals was rendered using Visual Molecular Dynamic program (VMD). According to the conceptual density functional theory, the Highest Occupied Molecular Orbital (HOMO) energies, Lowest Unoccupied Molecular Orbital (LUMO) energies, and the dipole moment (μ) magnitude were obtained. Besides the software quantified factors, other parameters including the energy gap between HOMO and LUMO (ΔE), mulliken electronegativity (χ); global hardness (γ), a fraction of transferred electrons from inhibitor molecule to metal surface (ΔN) (according to Koopmans's theory), ionization potential (I), electron affinity (E), global softness (σ), and electrophilicity

index (ω) of ionic liquids were calculated using following equations:

$$\Delta E = E_{LUMO} - E_{HOMO} \quad \text{(S1)}$$

$$\chi = \frac{-E_{LUMO} - E_{HOMO}}{2} \quad \text{(S2)}$$

$$\gamma = \frac{E_{LUMO} - E_{HOMO}}{2} \quad \text{(S3)}$$

$$\Delta N = \frac{(\chi_{Fe} - \chi)}{[2(\gamma_{Fe} + \gamma)]} \quad \text{(S4)}$$

$$I = -E_{HOMO} \quad \text{(S5)}$$

$$E = -E_{LUMO} \quad \text{(S6)}$$

$$\sigma = \frac{1}{\gamma} \quad \text{(S7)}$$

$$\omega = \frac{\chi^2}{2\gamma} \quad \text{(S8)}$$

where the theoretical values of γ_{Fe} and χ_{Fe} for iron are 0 eV mol^{-1} and 7 eV mol^{-1}, respectively.

Statistical analysis

The data were recorded as mean ± standard deviation for triplicate experiments. Analysis of variance (ANOVA) was carried out for statistical analysis by using SPSS 211 21.0 software. Tukey's test was used to analyze differences of the mean values 212 ($p < 0.05$).

References

1. X. He, L. Chen, Y. Tian, F. Ma, X. Huang and K. Cao, *Int. J. Electrochem. Sci.*, 2020, **15**, 12690-12705.

2. X. Zhou, H. Yang and F. Wang, *Electrochim. Acta*, 2011, **56**, 4268-4275.

3. M. Finsgar, S. Fassbender, S. Hirth and I. Milosev, *Mater. Chem. Phys.*, 2009, **116**, 198-206.

4. X. Li, H. Li, Z. Ling, D. Xu, T. You, Y.-Y. Wu and F. Xu, *Macromolecules*, 2020, **53**, 3284-3295.